WPJET1-CPR(17) 18247

FJR Nabais et al.

TAE stability calculations compared to TAE antenna results in JET

Preprint of Paper to be submitted for publication in Proceeding of 15th IAEA Technical Meeting on Energetic Particles in Magnetic Confinement Systems

This work has been carried out within the framework of the EUROfusion Consortium and has received funding from the Euratom research and training programme 2014-2018 under grant agreement No 633053. The views and opinions expressed herein do not necessarily reflect those of the European Commission.

TAE stability calculations compared to TAE antenna results in JET

F. Nabais[1], V. Aslanyan[2], D. Borba[1], R. Coelho[1], R. Dumont[3], J. Ferreira[1], A. Figueiredo[1], M. Fitzgerald[4], E. Lerche[4, 5], J. Mailloux[4], M. Mantsinen[6,7], P. Rodrigues[1], P. Puglia[8], S. E. Sharapov[4] and JET Contributors[§]

[§] *See the author list of "X. Litaudon et al 2017 Nucl. Fusion,* ***57****, 102001"*

EUROfusion Consortium, JET, Culham Science Centre, Abingdon, OX14 3DB, UK
[1]Instituto de Plasmas e Fusão Nuclear, Instituto Superior Técnico, Universidade de Lisboa, 1049-001 Lisboa, Portugal.
[2]MIT PSFC, 175 Albany Street, Cambridge, MA 02139, US
[3]CEA, IRFM, F-13108 Saint Paul Lez Durance, France
[4]CCFE, Culham Science Centre, Abingdon OX14 3DB, UK
[5]LPP-ERM/KMS, Association EUROFUSION-Belgian State, TEC partner, Brussels, Belgium
[6]Barcelona Supercomputing Center (BSC)
[7]ICREA, Pg. Lluís Companys 23, 08010 Barcelona, Spain.
[8]Ecole Polytechnique Fédérale de Lausanne (EPFL), Swiss Plasma Center (SPC), CH-1015 Lausanne, Switzerland

Abstract

The excitation of modes in the TAE gap by an external antenna can be modelled by a driven damped harmonic oscillator. By performing a frequency scan it is possible to determine the damping rate of the mode through the quality factor. This method has been employed in recent JET experiments dedicated to scenario development for the observation of alpha-driven instabilities in JET DT plasmas. However, the toroidal mode number *n* of the mode for which the measurements were performed could not be determined experimentally. The value of the damping obtained through experimental measurements for a selected time slice is then compared with those obtained from calculations performed by numerical codes for different modes with frequencies close to the experimental frequency of the antenna.

This paper describes the modelling method and presents the numerical simulations carried out using a suite of codes to calculate the damping of TAEs, which are compared with the value measured experimentally. The radial structure of these modes are first calculated with the ideal MHD code MISHKA. For each of these modes, the damping on thermal ions and thermal electrons and the contribution to the mode growth rate resulting from the resonant interaction with the ICRH accelerated ion population are calculated using the drift-kinetic code CASTOR-K. The radiative damping is calculated by using a complex resistivity in the resistive MHD code CASTOR code and the continuum damping is estimated using also the CASTOR code through the standard method of making the real part of the resistivity tend to zero. It was found the radiative damping is largely dominant over all other effects, except for

the n=3 TAE. The overall damping calculated numerically is consistent with the damping measured experimentally.

1. Introduction

In future fusion reactors, MHD modes like Toroidal Alfvén Eigenmodes (TAE) [1, 2] may lead to undesired redistribution of energetic ions, moving them away from the plasma core where they are needed to keep the plasma burning. Besides, if the energetic ions resonating with these TAEs are expelled from the plasma, they may cause serious damage to the chamber first wall and plasma facing components. It is then of great importance to have the capability to predict which modes are likely to be unstable in future tokamaks in order to develop the most favourable tokamak scenarios. Such capability must be tested in currently operating tokamaks, where the existence of real data makes it possible to compare the theoretical and numerical predictions with the experimental observations and measurements. The JET tokamak is particularly adequate to make such comparisons as it can operate with plasmas which under some aspects present close similarities with those expected for ITER.

TAE [1, 2] are modes with frequencies within the toroidicity gap existing in tokamak plasmas, which can be excited by the presence of energetic ion populations like those accelerated by Ion Cyclotron Resonance Heating (ICRH), injected by Neutral Beams (NBI) or alpha particles resulting from nuclear fusion reactions. For the modes to be destabilized, the drive originated from the interaction with the energetic ion population must overcome the overall damping coming from various origins. The main sources of damping are the collisional damping, the radiative damping, the continuum damping and the ion Landau damping on thermal species, both ion and electrons. In recent JET experiments dedicated to scenario development for the observation of alpha-driven instabilities in JET DT plasmas [3, 4], damping measurements using an external antenna have been obtained for three time slices corresponding to two different pulses. The method consists in modelling a driven damped harmonic oscillator so that a frequency scan makes possible to determine the damping rate through the quality factor. These measurements provided the opportunity to compare experimental results with the results obtained from calculations performed by a suitable set of numerical codes. From the existing damping measurements performed with the antenna, pulse #92416 was selected for a detailed numerical analysis. In this pulse, measurements were performed at two different time slices. The measurement performed at t=4.940 s, at a frequency of 174.76 kHz, resulted in a damping rate of γ/ω= -7.13% ± 1.74% while the

measurement performed at t=11.055 s, at a frequency of 218.3 kHz, resulted in a damping rate of γ/ω= -2.74% ± 0.54%. Since the frequency at which the first measurement was performed is not localized in the TAE gap, the second time slice was selected for a detailed analysis. Using the equilibrium reconstructed by EFIT or EFTF [5], the equilibrium refinement was performed by the equilibrium code HELENA [6]. The modes existing in the plasma with frequencies around the antenna frequency at t=11.055 s were calculated with the ideal MHD code MISHKA [7]. The different contributions to the overall growth rate of each mode were then accessed either with the resistive MHD code CASTOR [8] or with the drift-kinetic code CASTOR-K [9, 10].

This paper is organized as follows: In Section 2, a brief overview of pulse #92416 is given. In Section 3, a short description of the method used for measuring the damping rate is presented. In Section 4, the calculation of the mode eigenfunctions is performed using different sets of data. In Section 5, the different contributions to the overall damping rate are calculated and finally, in Section 6, the analysis of the results is done and conclusions are drawn.

2. Overview of pulse #92416

During last JET experimental campaign, a set of experiments dedicated to the development of a scenario for observation of alpha-driven TAE in the next JET DT experiments [3, 4] has been carried out. Pulse #92416 belonged to this set of experiments and its set up was designed envisaging the development of the afterglow scenario. The afterglow scenario in DT experiments is characterized by a sudden turning off of the NBI when a relevant population of alpha particles is present in the plasma. Since the stabilizing beam injected ions thermalize faster than the alpha particles, there is a window of time in which TAEs may be destabilized. In pulse #92416, ICRH was used and it continues to be applied after the NBI have been switched off. Figure 1 shows some relevant parameters of the discharge before and around the time at which the antenna measurement took place, t=11.055 s. The vertical dashed red line indicates the time at which the measurement was performed. It happened to be nearly coincident with a sawtooth crash which occurred at t=11.048 s. One should point out that the chord for which ECE measurements of the electron temperature are presented (bottom graphic of Figure 1) changed in radius with time as the magnetic field was also changing. This is the reason of the slow variation of T_e after t=9.0 s. This graphic is intended only to show the occurrence of sawtooth crashes.

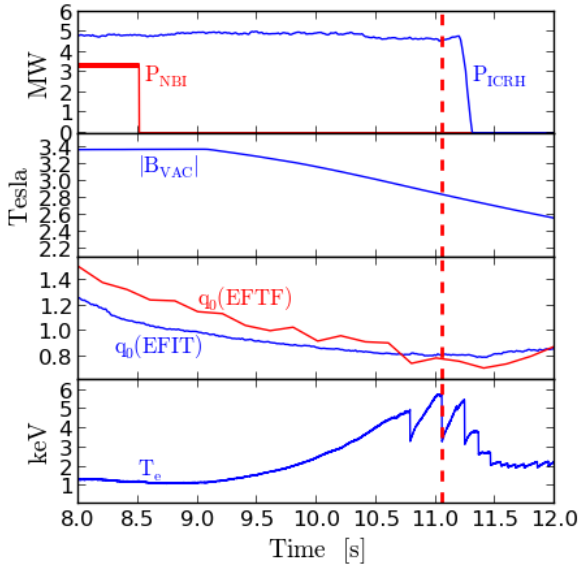

Figure 1: NBI and ICRH power, magnetic field, safety factor on axis calculated by EFIT and EFTF and electron temperature measured by ECE through chord 72 in the late phase of pulse #92416. The vertical dashed red line indicates the time at which the antenna measurement took place.

In this pulse the NBI (3.4 MW) was turned off at t=8.5 s, which corresponds to two and a half seconds before the antenna measurement took place. This means the neutral beam injected ion population has already thermalized at t=11.055 s, when the measurement took place. On the other hand, the ICRH (4.8 MW) was kept on until after t=11.055 s. Both EFIT and EFTF indicate that the safety factor on axis has already dropped below the unity at the time at which the measurement was performed. This is confirmed by measurements of electron temperature carried out with ECE which show the plasma sawtoothing after t=10.8 s. More information on this pulse can be obtained by looking at the magnetic spectrogram (see Figure 2).

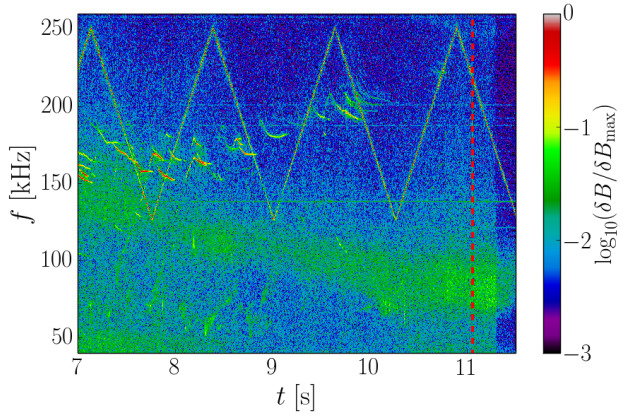

Figure 2: Magnetic spectrogram from Mirnov coils of the late phase of pulse #92416. The vertical dashed red line indicates the time at which antenna measurement took place.

Alfvén Cascades (AC) [11], also known as Reversed Shear Alfvén Eigenmodes (RSAE), are clearly visible up to t=9.5 s and seem to last, though less clearly, up to t=10.2 s, indicating the q-profile is reversed during this period. As the discharge progresses, the safety factor on axis gradually drops. First sawtooth crash is observed at around t=10.8s, indicating that at this time the safety factor on axis has already dropped below the unity, which is in agreement with both EFIT and EFTF. As the safety factor on axis drops, the q-profile eventually becomes monotonic. Both EFIT and EFTF indicate a monotonic q-profile at the time at which the antenna measurement took place (t=11.055 s). Finally, it is worth to note that after around t=10.2 s, all Alfvénic activity is supressed, with exception of a few short lived and very low amplitude modes at around t=10.7 s. This suggests the drive provided by the ICRH accelerated population was dwindling. At the time at which the antenna measurement took place, all Alfvénic modes were stable.

3. Alfvén Eigenmode Active Diagnostic

JET Alfvén Eigenmode Active Diagnostic (AEAD) [12, 13] is composed by two groups of four antennas each, both localized below the outboard midplane at opposite toroidal locations. Each AEAD antenna consists of a rectangular coil with 18 turns of inconel wire and are separated toroidally by 5º. In the last campaign the system went in operation and through an upgrade, it was the first time that more than four antennas have been powered simultaneously due to new amplifiers available. The frequency range of 125 kHz to 250 kHz was covered by the experiments. The toroidal mode number of the mode being probed was

not determined due to a reduced number of available magnetic probes during the experiment, which did not allow a precise n identification.

The antenna is used to excite/probe marginally stable modes and measures their damping rates as resonances in the magnetic probe signals as the antenna frequency is scanned across the resonant frequency. The measurement of the damping rate is based on the quality factor of the resonance, its width in frequency. The resonance measured in pulse #92416 at t=11.055 s is shown in the complex-plane in Figure 3. A transfer function [14] has been fitted to obtain a normalized damping rate of γ/ω = -2.74 ± 0.59%. A negative value of γ/ω indicates the mode is being damped while a positive value indicates the mode is growing in amplitude. The points shown in Figure 3 were collected during a 100 ms sweep and include points collected during the sawtooth crash at t=11.048 s, but there appear to be steady-state conditions. Indeed, most of points collected during the crash are clustered, i.e. there is no change in signal.

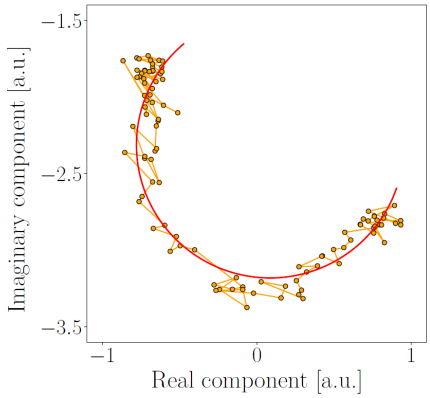

Figure 3: Magnetic probe signals of a resonance in pulse #92416, t=11.055 s. A transfer function [14] has been fitted to this data as shown.

4. Calculation of Eigenmodes

Since the identification of the toroidal mode number of the mode probed by the antenna was not possible, TAEs from n=3 to n=6, were considered as candidates. These are the toroidal mode numbers of the modes normally probed by the antenna. The first step in the workflow leading to the calculation of the structure of these modes is the reconstruction of the equilibrium. In JET, the equilibrium can be reconstructed by the codes EFIT, EFTF or EFTM [4]. These codes are similar, except they may use different sources of data. EFIT (Equilibrium FITting) is a numerical code that performs equilibrium reconstruction based on external diagnostics like external probes and magnetic coils. Since recent times, a high temporal

resolution EFIT is available at JET. EFTF is similar to EFIT but it also takes into account Faraday rotation measurements. In some cases, EFTF produces more accurate equilibria but in other cases, the equilibria obtained with EFIT are preferable. EFTM is similar to EFIT but it also uses internal data from Motional Stark Effect (MSE) diagnostic and it is usually seen as reconstructing the most reliable equilibria. However, at t=11.055 s MSE was not operating as the NBI had been already turned off. Since it is not known *a priori* which code yields a better equilibrium, at this stage both EFIT and EFTF were used in parallel. Due to the relatively low temporal resolution of EFTF, it happened the closest equilibrium was calculated for t=11.000 s, this is, before the sawtooth crash at t=11.048 s. On the other hand, the equilibrium reconstructed by EFIT was obtained for t=11.097 s, this is, after the crash. Nevertheless, equilibrium reconstruction based on external diagnostics are not much affected by internal events like sawtooth crashes. The second step of this workflow is the refinement of the equilibria reconstructed either by EFIT or EFTF. The equilibrium refinement was performed using the equilibrium code HELENA [5]. Finally, the TAEs radial structure are calculated by the ideal MHD MISHKA code [6]. Aside from the equilibrium, which is provided by HELENA, MISHKA also requires as input the mass density profile, on which the Alfvén frequency profile depends. The shape of the mass density profile was assumed to be similar to that of the electron density profile. Modes were calculated using density profiles from two distinct Thomson Scattering diagnostics, the High Resolution Thomson Scattering (HRTS) [15] and the LIDAR Thomson Scattering (LIDR) [16, 17]. The occurrence of a sawtooth crash so close from the time at which the antenna measurement took place may cause difficulties on the choice of the most adequate data to use in the simulations. A series of electron density profiles obtained with HRTS for time slices just before and after the occurrence of the sawtooth crash show that the effect of the crash on the profiles is not much significant. The maximum central density measured before the crash was close from n_e=3.9x10^{19}m^{-3}. In the simulations it was used a central value of n_e=3.68x10^{19}m^{-3} for the profile from LIDR and a central value of n_e=3.50x10^{19}m^{-3} for the profile from HRTS resulting from fitting the data. Figure 4 shows all the n=3 to n=6 modes calculated with MISHKA using the density profile from LIDR and the equilibrium reconstructed by EFIT.

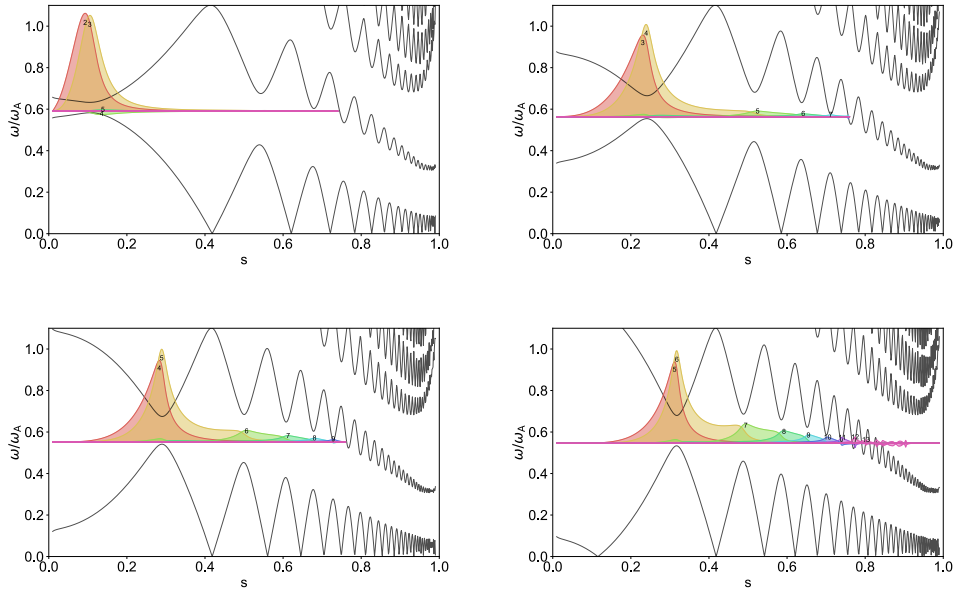

Figure 4: Radial structure of the n=3 to n=6 TAE calculated with MISHKA using data from LIDR and the equilibrium reconstructed by EFIT. Top left: n=3, top right: n=4, bottom left: n=5, bottom right: n=6.

The modes found with MISHKA code are composed by two dominant poloidal harmonics and are localized in the plasma core. Such modes are classified as core-localized TAEs [18,19]. These modes, when localized inside the q=1 surface, are known as tornado modes and have been extensively studied in JET [20, 21]. In pulse #92416 at t=11.055 s, ECE measurements found the sawtooth inversion radius localized at around s=0.40, which is in fair agreement with the location of the q=1 surface found by both EFIT and EFTF. Here, s is the square root of the normalized poloidal flux. So, all the modes found can be classified as tornado modes. It also apparent from Figure 4 that as the toroidal mode number increases, the calculated modes become radially localized at outer regions of the plasma and higher m poloidal harmonics increase in amplitude. However, the mode doesn't lose its core-localized nature. The n=5 modes calculated with different combinations of data (EFIT/EFTF) and (HRTS/LIDR) are shown in Figure 5. The radial structure of the n=5 mode is nearly identical when calculated using a density radial profile obtained either from HRTS or from LIDR. This result is not surprising as the density profiles obtained with both diagnostics are very similar except in the very centre of the plasma, where the electron density measured by HRTS is somewhat lower. This does not affect the radial structure of the calculated modes though it affects the Alfvén frequency in the centre of the plasma. The modes calculated with the equilibrium reconstructed by EFTF are radially localized slightly to the outside than those

calculated with the equilibrium reconstructed by EFIT. As consequence, the higher *m* poloidal harmonics also have higher amplitudes though the modes still keep their core-localized nature. The reason for this discrepancy in radial location steams from the transposition of the radial profiles measured in radius *R* to the square root of the normalized poloidal flux *s* as radial coordinate. Indeed, for the same radius *R* over the outboard midplane, EFTF associates a higher value of *s* than EFIT.

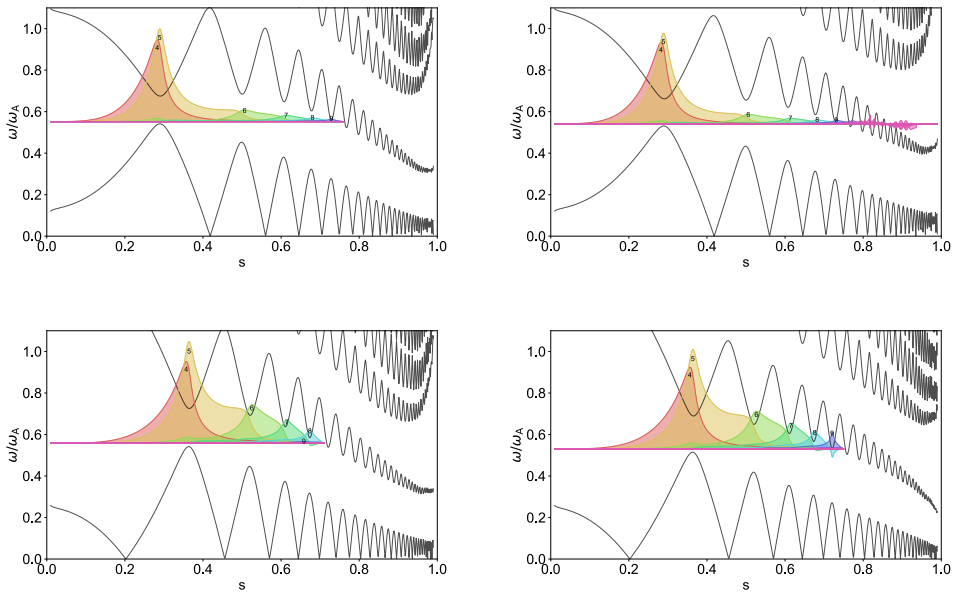

Figure 5: Radial structure of the n=5 mode calculated with MISHKA using different combinations of data. Top left: EFIT/LIDR, top right: EFIT/HRTS, bottom left: EFTF/LIDR, bottom right: EFTF/HRTS.

The frequencies of the modes calculated with the MISHKA code using the different combinations of data are presented in Table 1. These values compare with the antenna frequency at the time of the measurement, f=218.3 ± 0.8 kHz.

	EFIT/LIDR	EFIT/HRTS	EFTF/LIDR	EFTF/HRTS
n=3	f=227 kHz	f=232 kHz	f=232 kHz	f=225 kHz
n=4	f=217 kHz	f=219 kHz	f=218 kHz	f=214 kHz
n=5	f=212 kHz	f=214 kHz	f=213 kHz	f=209 kHz
n=6	f=210 kHz	f=210 kHz	f=211 kHz	f=208 kHz

Table 1: Frequencies of the modes calculated with MISHKA using different combinations of data.

The frequencies of the modes measured experimentally are affected by a Doppler shift due to plasma rotation. The Doppler shift depends linearly on the toroidal mode number and on the plasma rotation. Since the NBI was already turned off, there are no measurements of the plasma rotation at this time, t=11.055 s. However, since the main mechanism inducing plasma rotation in JET (and in other tokamaks as well) is the tangential injection of beam ions, this means the plasma rotation at t=11.055 s should be small. Without NBI, the plasma rotation in JET experiments is typically around 1 kHz. This is, for example, the frequency at which n=1 kink modes are commonly observed in experiments without NBI. Assuming the plasma is rotating with f_{rot}=1 kHz at the location of the modes, the shift in frequency of each mode due to the Doppler effect is then equal to its toroidal mode number ($\Delta f = n.f_{rot}$). Adding this frequency shift to the values of the mode frequencies calculated with MISHKA and presented in Table 1, the frequencies obtained for the n=5 mode nearly coincide with the frequency of the antenna. The frequencies obtained for the n=4 and n=6 modes are also very close. For the n=3 mode, the discrepancy between the calculated and the antenna frequencies is larger, but the difference is still relatively small, below 8%. Based on this, the mode probed by the antenna and for which the damping was measured is more likely to be an n=4, n=5 or n=6, though the possibility of being an n=3 should not be excluded.

5. Damping assessment

There are several damping mechanisms which may possibly affect the stability of the TAEs existing in the plasma, including the electron and ion Landau damping, the collisional damping, the continuum damping and the radiative damping. On the other hand, the only possible source of drive is provided by the population of energetic ions accelerated by ICRH. This population is responsible for the destabilization of several modes early on in the discharge up to around t=10.2 s, but the drive provided by the ICRH accelerated ion population has been dwindling over time in this late phase of the pulse. As it will be shown, at the time at which the antenna measurement was performed, t=11.055 s, the ICRH accelerated ion population is not driving the modes but it is actually damping them. Thus, all modes are necessarily stable at this time as there are no driving sources.

In this section, each of the terms contributing to the mode growth rate γ/ω are calculated separately. The contribution from the ICRH accelerated population to the mode growth rate and the electron and ion Landau damping are calculated using the CASTOR-K code [9, 10]. CASTOR-K is a drift-magnetic code which calculates the resonant exchange of energy

between populations of energetic or thermal particles and MHD modes, allowing this way to assess the drive/damping of the mode associated with this transference of energy. The collisional, continuum and radiative damping will be assessed using the resistive MHD stability code CASTOR [8]. Since, as mentioned, it is not known which mode was probed by the AEAD antenna, the calculations of drive/damping were performed for all the modes under consideration, n=3 to n=6, using by default the equilibrium reconstructed by EFIT and radial profiles from LIDR. In some cases, results using different sources of data (EFTF or HRTS) are also presented in order to evaluate how the results can be affected by the choice of the sources of data.

5.1 Collisional damping

The damping of TAEs may be enhanced due to collisions of trapped electrons with passing electrons and trapped electrons with ions [22], a mechanism which is usually known as collisional damping. This damping is habitually small and may become of relevance only for modes with high poloidal harmonics m. The collisional damping can be calculated using the CASTOR code taking the value of the resistivity at the radial position of the modes. CASTOR takes as input the normalized resistivity $\eta = \rho/(\mu_0 R_0 v_A(0))$, where ρ is the plasma resistivity, R_0 is the major radius of the magnetic axis, $v_A(0)$ is the Alfvén velocity at the magnetic axis, and μ_0 is the permeability of free space. To obtain the plasma resistivity it was used the Spitzer formula, $\rho \approx 2.8\text{x}10^{-8}/\ T_e^{3/2}$ (with T_e in keV) [23], which leads to values of the normalized resistivity between $\eta \approx 5\text{x}10^{-9}$ and 10^{-8}, depending on the modes. The values of the collisional damping obtained with CASTOR are presented in Table 2 for each of the modes considered. As it is apparent, the collisional damping is very small for all the modes under consideration.

$$n=3 \rightarrow (\gamma/\omega)_{coll} = -2.46 \text{ x } 10^{-4} \%$$
$$n=4 \rightarrow (\gamma/\omega)_{coll} = -1.03 \text{ x } 10^{-3} \%$$
$$n=5 \rightarrow (\gamma/\omega)_{coll} = -1.96 \text{ x } 10^{-3} \%$$
$$n=6 \rightarrow (\gamma/\omega)_{coll} = -5.35 \text{ x } 10^{-3} \%$$

Table 2: Collisional damping calculated with CASTOR using the equilibrium reconstructed by EFIT and radial profiles of n_e and T_e from LIDR.

5.2 Continuum damping

In ideal MHD, shear Alfvén eigenmodes may experience damping due to resonant interaction with the shear Alfvén continuum. This resonant power absorption occurs at the location where the frequency of the mode is the same as the frequency of a continuum branch. Effects such as charge separation and mode conversion occur at these resonances, resulting in damping known as continuum damping. A standard approach to calculate this damping numerically consists in representing these processes using a resistive magnetohdrodynamic (MHD) model. In these models, the continuum damping represents the limit of resistive damping as the resistivity vanishes [24]. The values of the continuum damping $(\gamma/\omega)_{cont}$ were estimated with the CASTOR code using this method. These values were found to be negligible for all the modes under consideration. This is not unexpected as all the modes have very small amplitudes at the location of the intersection with the Alfvén continuum. The continuum damping was also estimated using the eigenfunctions of the equilibrium reconstructed by EFTF instead of EFIT. These eigenfunctions are somewhat displaced to outer radial locations and could possibly lead to higher values of continuum damping. However, such was not the case. The values of the continuum damping obtained for the eigenfunctions solution of the equilibrium reconstructed by EFTF are also negligible.

5.3 Radiative damping

When adding non ideal effects like parallel electric field and first order finite Larmor radius terms to the ideal MHD model, the plasma perturbations are no longer Alfvén eigenmodes following the dispersion relation $\omega^2 = k_{=} v_A^2$ but become Kinetic Alfvén Waves (KAW) with a local dispersion relation $\omega^2 = k_{=} v_A^2 (1 + \zeta k_{\perp}^2 \rho_i^2)$. Here, $\zeta \equiv 3/4 + (T_e/T_i)[1 - i\delta(v_e)]$ is a complex number and $0 < \delta(v_e) \ll 1$ is a wave dissipation rate that depends on the electron collision frequency v_e and arises from the parallel resistivity model due to collisions between trapped electrons and passing particles [25]. Contrary to AEs, KAWs can propagate also transverse to the magnetic field. The fraction of the mode energy stored in parallel electric-field perturbation travels along the radial direction, thus leaving the resonant magnetic surface and being eventually transferred to the trapped-electron population by Landau damping. This damping mechanism is known as radiative damping of TAEs [25, 26]. The method followed to estimate the radiative damping [25] relies on the fact that exists a formal equivalence between a non-ideal MHD model that accounts for finite parallel electric field and first-order ion-gyroradius effects, and the resistive MHD model that is implemented in the CASTOR

eigenvalue code. Thus, the non-ideal effects can be simulated by introducing a complex resistivity in CASTOR. Since of the two components of non-ideal eigenmodes, KAWs suffer much stronger collisional damping than AEs, it is possible to infer the radiative damping by conducting a scan in $\delta(\nu_e)$ and obtaining the MHD damping rate as function of $\delta(\nu_e)$. A detailed explanation of this method is presented in references [27, 28].

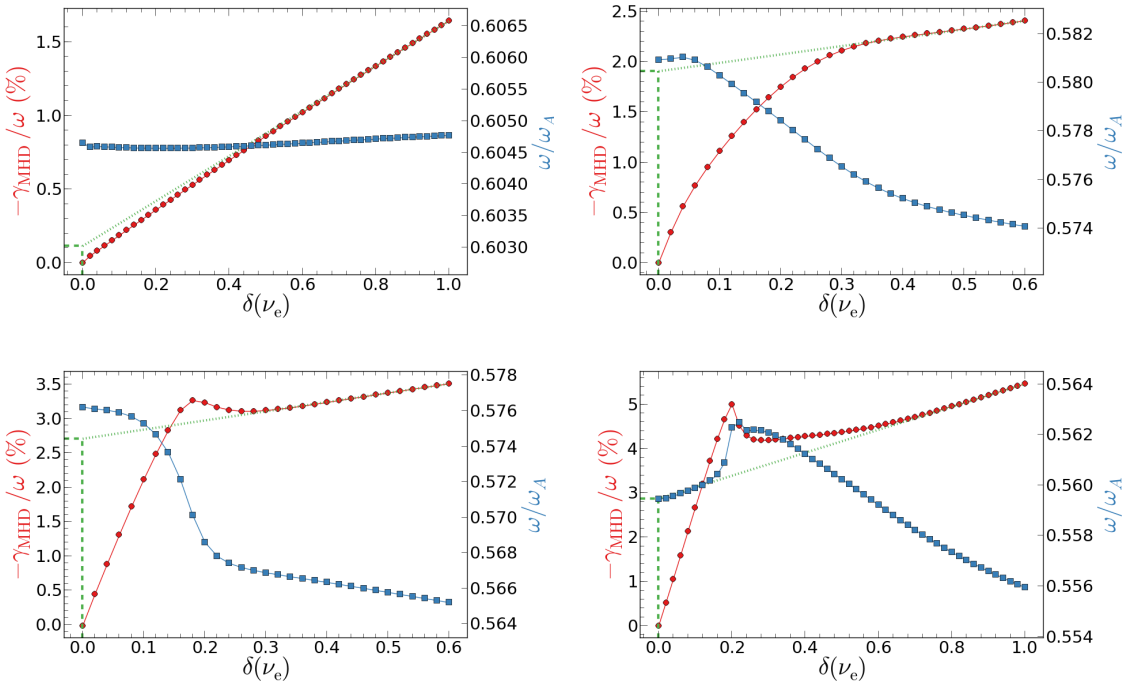

Figure 6: Estimation of the radiative damping rates for the n=3 (top left), n=4 (top right), n=5 (bottom left) and n=6 (bottom right) TAEs. Red curves represent the MHD damping rate calculated by CASTOR as a function of the wave dissipation rate whereas blue curves represent the frequency of the non-ideal eigenmode.

Figure 6 shows the results of the $\delta(\nu_e)$ scans performed with CASTOR. The values of the radiative damping obtained by linear fit analysis for each of the modes under consideration are summarized in Table 3. These results indicate the radiative damping is the dominant damping mechanism, except in the case of the n=3 mode which seems not to be much affected by radiative damping.

$n=3 \rightarrow (\gamma/\omega)_{rad} = -0.123\ \%$
$n=4 \rightarrow (\gamma/\omega)_{rad} = -1.91\ \%$
$n=5 \rightarrow (\gamma/\omega)_{rad} = -2.71\ \%$
$n=6 \rightarrow (\gamma/\omega)_{rad} = -2.87\ \%$

Table 3: Radiative damping calculated with CASTOR using the equilibrium reconstructed by EFIT and radial profiles of n_e and T_e from LIDR.

5.4 Ion and electron Landau damping

When a radial gradient of the thermal plasma density exists, the TAE may be damped by resonant interaction with the species composing the bulk plasma, which in this case are electrons and deuterium ions. The damping resulting from the resonant interaction between each of the thermal species and each of the Alfvén eigenmodes under consideration was calculated using the CASTOR-K code. In the case of electrons, the density and electron temperature profiles used in this simulation were obtained by fitting the data measured by LIDR. Just before the antenna measurement has taken place at t=11.055 s, a sawtooth crash has occurred at t=11.048 s with measurements from the fast temporal resolution ECE indicating a drop in the electron temperature in the centre of the plasma from around T_e=6 keV to T_e=3.5 keV. The value of the electron temperature in the centre of the plasma obtained from the fitting and used as input in CASTOR-K was T_e=4.2 keV, consistent with a swift partial recover of the electron temperature after the crash. The distribution of thermal electrons in the normalized magnetic moment $\Lambda \equiv \mu B/E$, where μ is the magnetic moment, was assumed to be isotropic. Since for the population of thermal deuterium ions no measurements of the radial density and temperature profiles are available, the profiles were assumed to be similar to those of the electrons. The distribution in Λ was assumed to be isotropic as well. In order to evaluate how the calculated damping depends on the choice of the sources of data, the calculation of the damping on thermal deuterium ions was also performed using the equilibrium reconstructed by EFTF and the profiles measured by HRTS instead of EFIT/LIDR. The values of the damping obtained are presented in Table 4.

Mode Number	Data	Int. Species	Damping
n=3	EFIT/LIDR	Ion (D)	γ/ω=-0.3822%
n=3	EFTF/HRTS	Ion (D)	γ/ω=-0.0311%
n=3	EFIT/LIDR	Electron	γ/ω=-0.0324%
n=4	EFIT/LIDR	Ion (D)	γ/ω=-0.0507%
n=4	EFTF/HRTS	Ion (D)	γ/ω=-0.0324%
n=4	EFIT/LIDR	Electron	γ/ω=-0.0216%
n=5	EFIT/LIDR	Ion (D)	γ/ω=-0.0517%
n=5	EFTF/HRTS	Ion (D)	γ/ω=-0.0334%
n=5	EFIT/LIDR	Electron	γ/ω=-0.0228%
n=6	EFIT/LIDR	Ion (D)	γ/ω=-0.0564%
n=6	EFTF/HRTS	Ion (D)	γ/ω=-0.0329%
n=6	EFIT/LIDR	Electron	γ/ω=-0.0262%

Table 4: Electron and ion Landau damping calculated with CASTOR-K.

The numerical results show the Landau damping is quite small in all cases except in the case of the n=3 mode solution of the equilibrium reconstructed by EFIT. This is due to the fact that this mode is localized much closer from the centre of the plasma than all others (see Figures 4 and 5). In this region, the density and temperature of the plasma are significantly higher leading to a larger Landau damping. In general, the values of the ion Landau damping calculated for the modes obtained using the equilibrium reconstructed by EFIT are higher than those calculated for the modes obtained using the equilibrium reconstructed by EFTF. This is also due to the localization of the modes, which in the first case are closer from the plasma centre. The simulations also show that low n TAEs are damped by strongly passing and passing ions (low Λ) and as the toroidal mode number of the modes increases, the damping contribution from trapped ions also increases. On the other hand, the damping of the TAEs on electrons is due to resonant interaction with trapped electrons.

5.5 Contribution to γ/ω from the ICRH minority population

At t=11.055 s, the plasma still contains a significant population of hydrogen minority ions accelerated by ICRH which may experience a resonant interaction with the TAEs. The contribution to the modes growth rate coming from this resonant interaction has been calculated using the CASTOR-K code. In this code, the distribution function of the energetic

ion population is inputted as function of the radial density (from which the toroidal canonical momentum P_φ is obtained), the energy E and the normalized magnetic moment Λ. Normally, the ICRH is applied on-axis, which was the case of pulse #92416 during the current flat-top phase. For on-axis heating, the ICRH accelerated population distribution is peaked near the plasma centre and the ions efficiently accelerated by ICRH are those moving in banana orbits which tips fall over the ICRH resonant layer. A common approximation is to assume the whole energetic ion population to be characterized by a single Λ, which is given by the ratio between the major radius of the resonant layer and the magnetic radius $\Lambda=R_{res}/R_0$. Thus, for on-axis heating, the whole energetic ion population is characterized by Λ=1.

In the case under analysis, the AEAD antenna measurement was performed late on the discharge and at the time at which measurement was performed (t=11.055 s), the magnetic field was already ramping down (see Figure 1), implying the ICRH resonance layer was moving inward in major radius. At t=11.055 s, the ICRH resonance layer was localized at R_{res}=2.559 m which, over the midplane, corresponds to s=0.517 and R_{res}/R_0=0.865. The radial distributions of the energetic ion density and temperature have been calculated both with the PION code [29] and with the 2D full-wave CYRANO code [30]. CYRANO founds a radial distribution of energetic ions steeply peaked and centred near the magnetic flux surface which is crossed by the ICRH resonant layer over the midplane. This code, which uses the Stix model [31], predicts the energetic ion temperature to peak around the same location as the density, reaching a maximum temperature of T_{HOT}=50 keV at the peak. On the other hand, PION predicts the energetic ion density profile to be less steeped and peaked much closer from the core, at around s=0.35. The energetic ion temperature predicted by PION goes up to T_{HOT} =190 keV on its peak.

The effects of the resonant interaction between the ICRH accelerated ion population and the TAEs under consideration calculated by CASTOR-K are presented in Table 5. For these results, it was used the energetic ion distribution function calculated by CYRANO, the mass density profile obtained with data from LIDR and the equilibrium reconstructed by EFIT.

$$n=3 \rightarrow (\gamma/\omega)_{ICRH} = -1.61 \times 10^{-5}\ \%$$
$$n=4 \rightarrow (\gamma/\omega)_{ICRH} = -3.0 \times 10^{-3}\ \%$$
$$n=5 \rightarrow (\gamma/\omega)_{ICRH} = -0.025\ \%$$
$$n=6 \rightarrow (\gamma/\omega)_{ICRH} = -0.09\ \%$$

Table 5: Contribution to the TAEs growth rate resulting from the resonant interaction with the ICRH accelerated population as calculated with CASTOR-K. The energetic ion distribution was calculated by CYRANO, the equilibrium was reconstructed by EFIT and mass density profile was obtained from LIDR data.

Results presented in Table 5 show that the off-axis ICRH accelerated population is not transferring energy to any of the TAEs, but instead it is actually damping the modes. Results from Table 5 are easily understandable. The modes are being damped instead of driven because the energetic ion population peaks at an outer location than modes so the resonant interaction occurs in a region where the radial density gradient is positive. The damping is small because the modes are far apart from the peak of the energetic ion distribution function, and the damping increases with the toroidal mode number because modes with higher *n* are localized closer from the peak of the energetic ion density. If the energetic ion population calculated by PION is considered instead of that from CYRANO, then the modes become localized in a region of high density of energetic ions and the damping becomes much higher, up to around $(\gamma/\omega)_{ICRH} = -3.0\ \%$ for the modes with the highest damping.

6. Summary and conclusions

The damping of a TAE mode was measured in pulse #92461 at t=11.055 s using the new AEAD JET antennas. This value was compared with the results from numerical calculations which include all possible relevant sources of damping/drive obtained by using different sets of numerical codes. These include the collisional damping, radiative damping, continuum damping, Landau damping on thermal species and resonant interaction with the ICRH accelerated population. Since the toroidal mode number of the TAE for which the measurement was performed could not be determined experimentally, calculations were performed for a range of modes with toroidal mode numbers between n=3 and n=6. The radial structure of the modes calculated with the MISHKA code indicates these modes are core-

localized TAE inside the q=1 surface (tornado modes). The agreement between the experimental frequency of the mode probed by the antenna and the frequency of the modes calculated by MISHKA is very good.

The damping calculations show that the radiative damping is largely dominant over all other sources of damping except for the n=3 TAE, for which the radiative damping is small. The off-axis ICRH accelerated population was found to be also damping the TAEs instead of driving. Continuum damping, collisional damping and ion and electron Landau damping were found to be very small, except the ion Landau for the n=3 TAE, as this mode is localized close from the centre in a region where the thermal density and temperature are higher. Table 6 shows the overall damping obtained for each mode, taking into account all considered sources of damping.

n=3 → γ/ω = -0.50 %
n=4 → γ/ω= -1.96 %
n=5 → γ/ω = -2.79 %
n=6 → γ/ω = -3.01 %

Table 6: Overall damping rate for each mode taking into account all considered sources of damping. Data used is from EFIT/LIDR and energetic ion distribution function from CYRANO.

The damping rate measured by the antenna is γ/ω = -2.74 ± 0.59%. The agreement in frequency and calculated damping is very good for the n=5 and n=6 TAEs, one of these being probably the mode probed by the antenna. The measured damping is basically radiative damping.

References

[1]- Cheng C. and M. S. Chance 1986 *Phys. Fluids* **29** 3695
[2]- Wong K.-L. 1999 *Plasma Phys. Control. Fusion* **41** R1
[3]- Mailloux J. *et al*. "*Plasma preparation for alpha-particle excitation of TAEs in JET DT plasmas*", presented at 44th EPS Conference, June 2017, Belfast, North Ireland
[4]- Dumont R. *et al*. "*Scenario development for the observation of alpha-driven instabilities in JET DT plasmas*", submitted to *Nucl. Fusion* (Special Issue)
[5]- Lao L.L. *et al*.1985 *Nucl. Fusion* **25** 1611
[6]- Huysmans L.G. *et al.* 1993 *Phys. Fluids B* **5** 1545
[7]- Mikhailovskii A.B. *et al.* 1997 *Plasma Phys. Rep.* **23** 844
[8]- Kerner W. *et al*. 1998 *J. Comput. Phys*. **142** 271
[9]- Borba D. *et al*. 1999 *J. Comput. Phys.* **153** 101
[10]- Nabais F. *et al*. 2015 *Plasma Sci. Technol*. **17** 89

[11]- Sharapov S.E. *et al*. 2002 *Phys. Plasmas* **9** 2027
[12]- Aslanyan V. *et al*. "*Progress and first measurements from the upgraded Alfvén Eigenmode Active Diagnostic on JET*", presented at 44th EPS Conference, June 2017, Belfast, North Ireland
[13]- Puglia P. *et al*. 2016 Nucl. Fusion **56** 112020
[14]- Fasoli A. *et al*. 1995 *Phys. Rev. Lett*. **75** 645
[15]- Frassinetti L. *et al*. 2012 *Rev. Sci. Instrum*. **83** 013505
[16]- Salzmann H. *et al*. 1988 *Rev. Sci. Instrum*. **59** 1451
[17]- Maslov M. *et al*. 2013 *JINST* **8** C11009
[18]- Berk H. *et al* 1995 *Phys. Plasmas* **2** 3401
[19]- Fu G.Y. *et al*. 1995 *Phys*. Plasmas **2** 1029
[20]- Nabais F. *et al.* 2010 *Nucl. Fusion* **50** 115006
[21]- Nabais F. *et al.* 2012 *Nucl. Fusion* **52** 083021
[22]- Gorelenkov N.N. and Sharapov S.E. 1992 *Physica Scripta* **45** 163
[23]- J. Wesson, "*Tokamaks*" 1997 Oxford University Press, Oxford
[24]- Bowden G. W. *et al*. 2014 *Physics of Plasmas* **21** 052508
[25]- Candy J. and Rosenbluth M.N. 1994 *Phys. Plasmas* **1** 356–372
[26]- Mett R.R. and Mahajan S.M. 1992 *Phys. Fluids B* **4** 2885–2893
[27]- Rodrigues P. *et al*. 2015 *Nucl. Fusion* **55** 083003
[28]- Figueiredo A. *et al*. 2016 *Nucl. Fusion* **56** 076007
[29]- Eriksson L-G. *et al*. 1993 *Nucl. Fusion* **33** 1037
[30]- Lerche E. *et al.* 2009 *Plasma Phys. Control. Fusion* **51** 044006
[31]- Stix T.H. *Nucl. Fusion* 1975 **15** 737

Acknowledgments – This work has been carried out within the framework of the EUROfusion Consortium and has received funding from the Euratom research and training programme 2014-2018 under grant agreement No 633053. IST activities also received financial support from "Fundação para a Ciência e Tecnologia" through project UID/FIS/50010/2013. The views and opinions expressed herein do not necessarily reflect those of the European Commission.